Technical Note

Catastrophe Instability Mechanism of the Pillar-Roof System in Gypsum Mines Due to the Influence of Relative Humidity

Kaizong Xia[1]; Congxin Chen[2]; Yichao Zhou[3]; Xiumin Liu[4]; Yun Zheng[5]; and Yucong Pan[6]

Abstract: In this study, a simplified mechanical model is proposed based on the failure characteristics of a gypsum pillar–roof system obtained through *in situ* investigation. Then, a cusp catastrophe model for the gypsum pillar–roof system is established based on the given stress–strain relations of the gypsum rock. Using this model, the instability mechanism for the gypsum pillar–roof system is investigated. The results of the analysis indicate that the stress–strain relation of gypsum rock derived from damage mechanics theory can accurately describe its strain-softening behavior after the peak stress and that increases in the relative humidity around a pillar or both a pillar and the roof bed can increase the stiffness ratio of the support system and consequently result in a more stable support system. However, if the relative humidity around the roof bed increases, the stiffness ratio of the system decreases, increasing the possibility of catastrophic failure of the support system. The case study revealed that the influence of the relative humidity on the support system is significant, higher relative humidity in the mine's atmosphere increases the probability of instability in the support system, and the influence of the relative humidity change around the pillar on system stability is greater than that around the roof bed. **DOI: [10.1061/(ASCE)GM.1943-5622.0001378](https://doi.org/10.1061/(ASCE)GM.1943-5622.0001378).** © *2019 American Society of Civil Engineers.*

Author keywords: Gypsum mine; Catastrophe model; Relative humidity; Pillar; Roof bed.

Introduction

Rock masses of the roof in gypsum mines are often weak mudstones, siltstones, or similar lithologies with extensive joints and fractures that easily induce undesirable caving problems. Although few fiber gypsum mines have adopted the long-wall fill stopping or room-and-pillar fill stopping methods, the majority of mining engineering projects are still undertaken using the room-and-pillar mining method (Auvray et al. 2004, 2008; Wang et al. 2008a, b; Bertolini

[1]Assistant Professor, State Key Laboratory of Geomechanics and Geotechnical Engineering, Institute of Rock and Soil Mechanics, Chinese Academy of Sciences, Wuhan, Hubei 430071, PR China; formerly, Univ. of Chinese Academy of Sciences, Beijing 100049, PR China (corresponding author). Email: xiakaizong1988@sina.com

[2]Professor, State Key Laboratory of Geomechanics and Geotechnical Engineering, Institute of Rock and Soil Mechanics, Chinese Academy of Sciences, Wuhan, Hubei 430071, PR China. Email: cxchen@whrsm.ac.cn

[3]Lecturer, School of Civil Engineering, Changsha Univ. of Science and Technology, Changsha 410076, China. Email: zhouyichao1@126.com

[4]Associate Professor, State Key Laboratory of Geomechanics and Geotechnical Engineering, Institute of Rock and Soil Mechanics, Chinese Academy of Sciences, Wuhan, Hubei 430071, PR China. Email: xmliu@whrsm.ac.cn

[5]Assistant Professor, State Key Laboratory of Geomechanics and Geotechnical Engineering, Institute of Rock and Soil Mechanics, Chinese Academy of Sciences, Wuhan, Hubei 430071, PR China. Email: yzheng@whrsm.ac.cn

[6]Postdoctoral Researcher, Key Laboratory of Safety for Geotechnical and Structural Engineering of Hubei Province School of Civil Engineering, Wuhan Univ., Wuhan, Hubei 430072, PR China. Email: pyc1991@whu.edu.cn

et al. 2010; Castellanza et al. 2010; Cui et al. 2014). During ore extraction, a certain thickness of gypsum rock above the mined-out area should be set to increase the stability of the superincumbent strata; under these conditions, the roof bed and pillars, both composed of gypsum rock, act together as a support system for the mined-out area. Large masses of undealt mined-out areas have gradually accumulated as the mining depth increases, and the mined-out areas have become considerably less stable. Collapses of the mined void and cavings of the superincumbent strata occur frequently (Yilmaz 2007; Wang et al. 2008a, b). Such collapses have become the primary hazards of nonmetal mines in China and have resulted in personal injury, road damage and building collapse; these collapses can cause serious losses to the economy, to society and to the environment (Table 1). Generally, these accidents depend on the mine conditions, the extraction ratio, and the depth of the mine, among other factors, but one of the unavoidable reasons for these accidents is the softening effect of gypsum rock via the absorption of excess water in the mine atmosphere (Yilmaz 2007; Wang et al. 2008a; Yilmaz and Yuksek 2009), which greatly degrades the mechanical properties of the pillar–roof support system. Therefore, to reduce the risk of accidents, an analysis of the stability of the mined-out areas in a gypsum mine must consider the behavior of gypsum rock as it relates to changes in relative humidity.

As many researchers have noted, deformation failure of the pillar–roof system in gypsum mines is a complex, nonlinear, irreversible evolutionary process. Under the influences of the stress state and other environmental factors, deformation of the pillar–roof system changes from the slow stable continuous stage to the sudden unstable failure stage (Wang et al. 2008a, b; Bertolini et al. 2010; Castellanza et al. 2010). Catastrophe theory is a mathematical technique that was developed principally by the French mathematician Thom (1972) to model natural phenomena, and the established concept emphasizes the nonlinear, irreversible, and dynamic process of the support system (Thom 1972; Henley 1976; Saunders 1980; Qin et al. 2001a, b, 2006). Many researchers have employed catastrophe theory to study the stability of mined-out areas in coal

and metal mines, and many useful results have been reported in practical engineering projects (Hu et al. 2005; Wang et al. 2006; Pan et al. 2009; Liu et al. 2013) that illustrate the effectiveness of the stability analysis of mined-out areas using catastrophe theory. In this study, a cusp catastrophe model for the gypsum pillar–roof system is established based on the stress–strain relations of gypsum rock in uniaxial compression tests at different relative humidities and a simplified model of system mechanics. The instability mechanisms for the gypsum pillar–roof system under the effect of relative humidity were investigated using the proposed model.

Stress–Strain Behavior of Gypsum Rock under Different Relative Humidities

Stress–strain Relation

Fig. 1 presents the stress–strain curves of the gypsum rock specimens under the natural condition or under wet conditions with relative humidities of 70, 85, and 100%. Clearly, the strain-softening phenomenon of the gypsum rock specimen is easily detectable, and its constitutive behavior exhibits strain softening. Many researchers have suggested that damage mechanics theory can well describe the inherent mechanism of this type of stress–strain relation (Wang et al. 2006; Pan et al. 2009; Cheng et al. 2017; Wang et al. 2017). Hence, the constitutive model of the gypsum rock under uniaxial stress conditions can be expressed as

$$\sigma = E_0\varepsilon[1 - D(\varepsilon)] \tag{1}$$

where σ, E_0, and ε = stress, initial elastic modulus, and compressive strain of the gypsum rock specimen, respectively; and $D(\varepsilon)$ = damage parameter. Because the widely accepted strength distribution identified with rock failure applications is the Weibull distribution (Wang et al. 2006; Pan et al. 2009), the Weibull distribution law is employed to describe the stress–strain relation of gypsum rock in this study. That is

$$\sigma = E_0\varepsilon \exp\left[-\left(\frac{\varepsilon}{\varepsilon_0}\right)^m\right] \tag{2}$$

$$D(\varepsilon) = 1 - \exp\left[-\left(\frac{\varepsilon}{\varepsilon_0}\right)^m\right] \tag{3}$$

where ε_0 = the average strain; and m = the shape parameter that allows this function to consider a wide variety of shapes. A larger index m indicates more homogeneous properties and brittleness of the rock; thus, m can be referred to as a homogeneity index or brittleness index (Tang 1997; Wang et al. 2006).

Relationship between Mechanical Parameters and Relative Humidity

The mechanical parameters on gypsum rock specimens under different relative humidities are presented in Table 2. Compared with the natural condition, the mechanical parameters of gypsum rock specimens show significant softening characteristics, and the strength and deformation parameters are greatly reduced. As the relative humidity in the mine atmosphere increases from the natural condition to a relative humidity of 100%, the values of the elasticity modulus and the unconfined compressive strength of the gypsum rock decrease by 12.7 and 16.3%, respectively. The reason for these

decreases is that gypsum rock is subjected to dissolution and recrystallization upon the absorption of water from the mine atmosphere, thereby causing mineral loss and causing the rock structure to become looser and more porous, and thus degrading its mechanical parameters to some extent. The phenomenon by which the chemical effect of absorption of water by gypsum rock results in partial loss of its strength is known as the water-softening effect. The functional form to describe the water-softening effect for different rocks can be obtained by test data fitting.

Eq. (2) indicates that the expression of the constitutive relation of gypsum rock includes three variables: the initial elastic modulus E_0; the average strain ε_0; and the brittleness index m. These three variables will change to some extent under different relative humidities. However, as illustrated in Table 2, the average strain ε_0 remains nearly constant at 6.0×10^{-3}, the initial elastic modulus E_0 gradually decreases from 6.59 to 5.75 MPa, and the brittleness index m also gradually decreases from 1.62 to 0.90. Hence, in this study, the influence of the relative humidity of the mine atmosphere on the constitutive relation of gypsum rock is investigated in terms of the initial elastic modulus E_0 and brittleness index m. Defining $g_1'(w)$ as the water-softening function of the initial elastic modulus E_0 and $g_2'(w)$ as the water-softening function of the brittleness index m, the constitutive relation of gypsum rock can be rewritten

$$\sigma' = g_1'(w)E_0\varepsilon \exp\left[-\left(\frac{\varepsilon}{\varepsilon_0}\right)^{g_2'(w)m}\right] \tag{4}$$

According to the values of the initial elastic modulus E_0 and the brittleness index m in Table 2, the water-softening functions of the initial elastic modulus E_0 and the brittleness index m for different relative humidities are illustrated in Figs. 2(a) and 2(b). Clearly, the water-softening functions of the initial elastic modulus E_0 and the brittleness index m can be expressed as power and linear functions, respectively ($R = 0.9837$ and 0.9402, respectively), and $g_1'(w)$ and $g_2'(w)$ are both equal to 1 under natural conditions.

Cusp Catastrophe Model of the System Instability

Mechanical Model

According to *in situ* investigations of the mined-out area in many gypsum mines, the distribution characteristics of such mines are illustrated in Fig. 3. In Fig. 3, the size of a pillar is $w_p \times l_p$, where w_p denotes its width perpendicular to the advance direction and l_p denotes its length parallel to the advance direction. The spacings between adjacent pillars perpendicular to and along the advance direction are $(w_0 + w_p)$ and $(k + k)$, respectively.

The stability analysis of the mined-out area is a complex three-dimensional (3D) problem. For simplicity, many researchers have assumed that the length of the mined-out area is significantly greater than its width and that the number of mined voids is infinite based on the principle of physical independence of forces; in this manner, the effect of the boundary and span (with the boundary defined as the rock masses above the left and right corners of the mined-out area) can be neglected. The pillars exert a set of uniform supporting forces on the roof bed; as a result, the complex 3D problem of calculating the roof thickness can be simplified to an ideal elastic plane problem. On this basis, in this study the uniform loadings on the roof bed exerted by the pillars are regarded as an equivalent concentration force acting on the center point; thus, a simplified
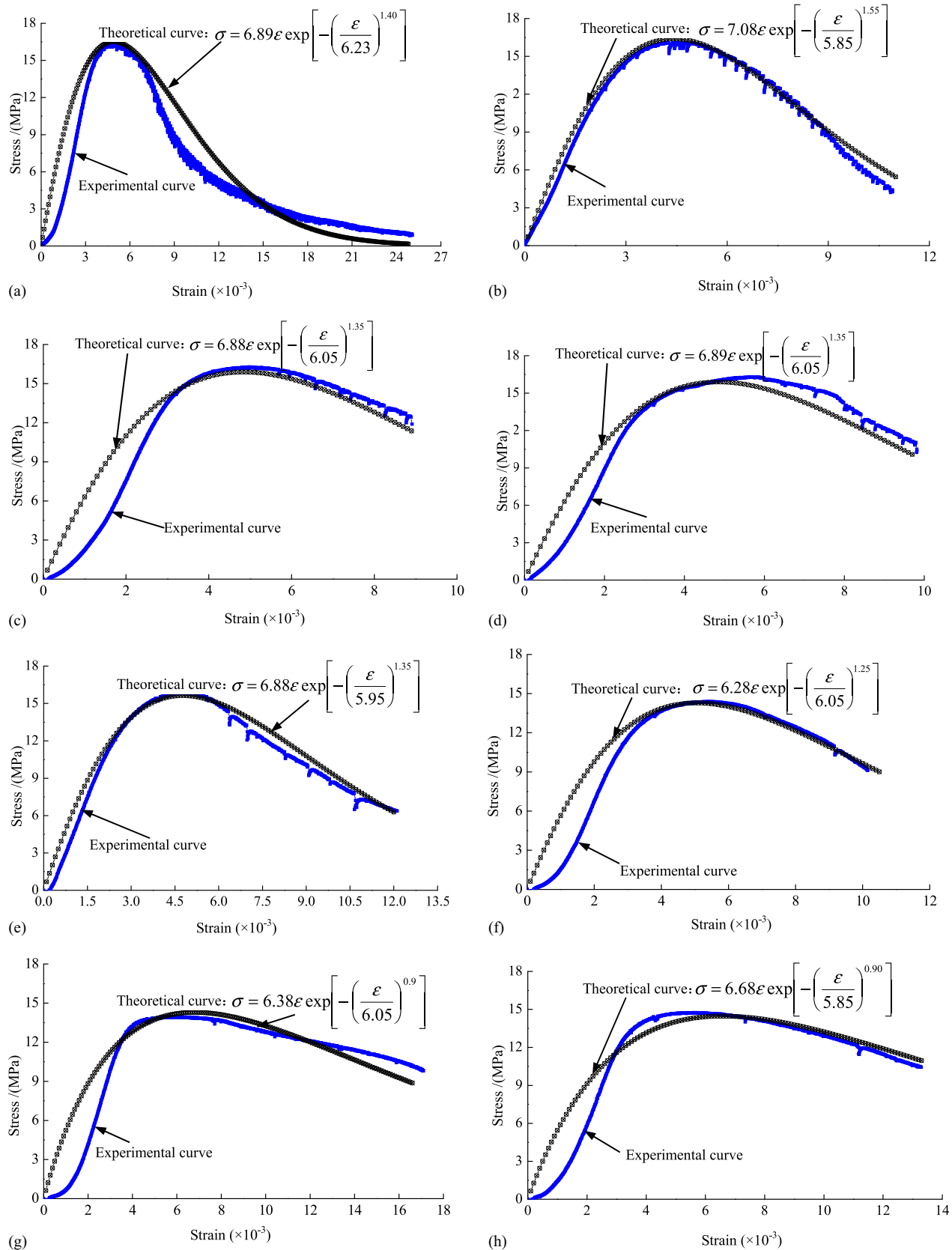
Fig. 1. Experimental and theoretical curves of gypsum rock specimens under uniaxial compression: (a) natural specimen No. 1-1; (b) natural specimen No. 1-2; (c) specimen No. 2-1 with a relative humidity of 70%; (d) specimen No. 2-2 with a relative humidity of 70%; (e) specimen No. 3-1 with a relative humidity of 85%; (f) specimen No. 3-2 with a relative humidity of 85%; (g) specimen No. 4-1 with a relative humidity of 100%; and (h) specimen No. 4-2 with a relative humidity of 100%.

Table 1. Typical disasters at gypsum mines in China

Name of mine	Date of accident	Number of deaths	Collapse area, economic loss
Pingyi Gypsum Mine in Shangdong Province	December 25, 2015	19 miners buried underground	Cracking and collapse in adjacent residential areas, roads, and agricultural land and an induced earthquake ($M = 4.0$)
Guanyuan Gypsum Mine in Jiangshu Province	April 15, 2012	10 miners trapped underground	Ground subsidence for more than 7,000 m^2, cracks in the traffic lines near the mining area with a maximum opening of 20 cm
Shangwangzhuang Gypsum Mine in Hebei Province	November 6, 2005	37 lives lost, 32 miners injured	53,000-m^2 collapse area, 480,000-m^2 movement area, collapse of 88 buildings, direct economic loss of 7.74 million yuan
Tiande Gypsum Mine in Hunan Province	August 19, 2006	9 lives lost	Collapse area of approximately 18,000 m^2
Henda Gypsum Mine in Guangxi Province	May 18, 2001	29 lives lost	Direct economic loss of 4.56 million yuan
Jinmen Gypsum Mine in Hubei Province	Since 2005	No deaths	33 ground collapses, collapse area of 387,000 m^2

Table 2. Mechanical parameters of gypsum rock specimens under different relative humidities

Specimen condition	Unconfined compressive strength [σ_c (MPa)]	Elastic modulus [E (GPa)]	Initial elastic modulus [E_0 (GPa)]	Average strain [ε_0 ($\times 10^{-3}$)]	Brittleness index m
Natural condition	17.14	6.59	7.19	5.9683	1.62
Relative humidity of 70%	16.27	6.26	6.88	6.0519	1.35
Relative humidity of 85%	15.12	6.00	6.58	6.0019	1.30
Relative humidity of 100%	14.35	5.75	6.53	5.9519	0.90

mechanical model of the gypsum pillar–roof system, as illustrated in Fig. 4, is chosen from Profile I–I, which contains one unit of three pillars. Here, the roof bed can be simplified to a beam with flexural stiffness EI, and its self-weight and the load of the overburden strata can be simplified to a uniform loading density q.

Generally, the instability of the mined-out area can be mainly attributed to the instability of the pillars and the roof bed, particularly the pillars' instability. This conclusion can also be reached based on the in situ investigation of many gypsum mines in Hunan, Hebei, Guangxi, and Shandong Provinces in China as well as in the case analyses of several major accidents. Moreover, the results of numerical modeling also reveal that the main reason for the collapse of the mined-out areas in gypsum mines is the pillars' instability. Generally, failure due to pillar instability can be generally attributed to the unfavorable effects of frequent blasting, loading, and unloading, water softening, or the decrease in pillar size caused by human activities. Furthermore, because the unfavorable effects on different pillars often vary widely, the collapse of the mined-out area in a gypsum mine will generally begin with the local destruction of the key pillar under the most severe conditions, at which point pillar collapse transfers the load onto the surrounding pillars. This process, in turn, may damage the other pillars, thus inducing a "domino effect" (Hoek and Brown 1980). Finally, a large-area collapse of the roof bed occurs; in the worst case, ground collapse may occur over the entire mined-out area (Wang et al. 2008a, b). If it is assumed that the primary failure occurs in pillar B (Fig. 4) and the roof bed remains in the elastic state during the pillar failure process, only releasing the energy without failure, then the simplified analysis model can be established as given in Fig. 5.

As a preliminary analysis, it is suggested that the constitutive relation of the gypsum rock can approximately represent the constitutive relation of the pillars. The load acting on the pillar is

$F = \sigma'A$, and the pillar axial deformation is $u = \varepsilon H$, where A denotes the cross sectional area of the pillar and H denotes the pillar height. Thus, coupled with Eq. (4), the following equation can be given:

$$
F = \sigma'A = g'_1(w)\frac{E_0 A}{H}u\exp\left[-\left(\frac{u}{u_0}\right)^{g'_2(w)m}\right]
$$

$$
= g'_1(w)\lambda u\exp\left[-\left(\frac{u}{u_0}\right)^{g'_2(w)m}\right] \tag{5}
$$

where $\lambda = E_0 A/H$ denotes the initial stiffness of the pillar. Solving $F'' = 0$ shows that the curve of Eq. (5) has one inflection point at $u = u_1 = u_0\left[g'_2(w)m + 1/g'_2(w)m\right]^{1/[g'_2(w)m]}$. Substituting $u = u_1 = u_0\left[g'_2(w)m + 1/g'_2(w)m\right]^{1/[g'_2(w)m]}$ into $F' = 0$, shows that the absolute slope of the function in Eq. (5) is $\lambda_1 = g'_1(w)\lambda g'_2(w)m \exp\left\{-\left[g'_2(w)m + 1/g'_2(w)m\right]\right\}$.

Equation for the Deflection Curve of the Roof Bed

Because it is extremely complex to obtain the supporting force and bending moment at the ends of pillars A and C, Pan et al. (2009) proposed using the displacement method of structural mechanics to investigate the instability mechanism for a rock beam–narrow coal pillar system in which the end of the rock beam is fixed to the unmined coal seam; such a method is employed in this study. Based on the assumed mechanical model illustrated in Fig. 4, the deflection curve of the roof bed exhibits a continuous half-wave shape between each of the two pillars under the pillar support, and the rotation angle of the ends of

(b)

(c)
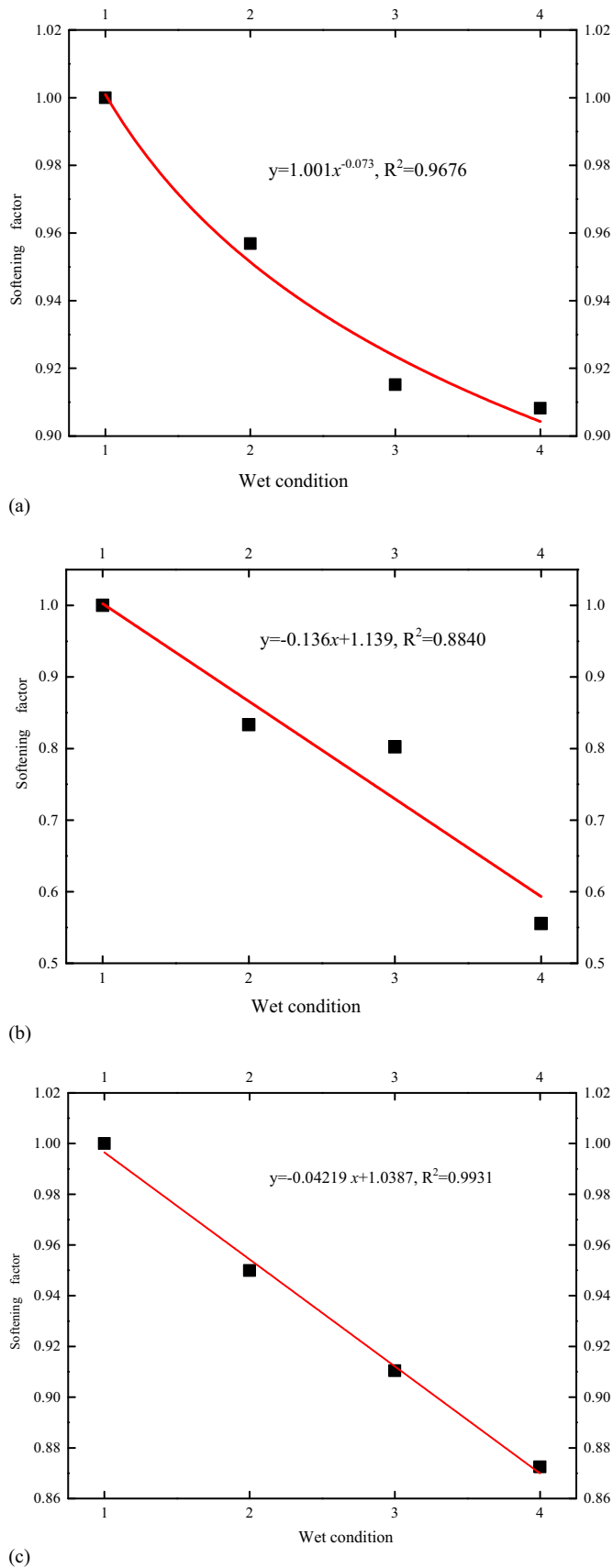
Fig. 2. Water-softening function by fitting laboratory test data (numbers 1, 2, 3, and 4 in x-coordinate refer to the natural condition and wet conditions with relative humidities of 70, 85, and 100%, respectively): (a) initial elastic modulus E_0; (b) brittleness index m; and (c) elastic modulus E.

pillars A and C should be equal to zero. Under the equivalent uniform load q, the pillar displacement at its upper end can be assumed to be u, equal to the vertical deflection at the middle point of the roof bed (Fig. 6). As a result, the moment M_{AB} (counterclockwise moments are positive) and shear force Q_{AB} at the end A of the roof bed can be obtained as

$$
\left.
\begin{aligned}
M_{AB} &= -\frac{ql^2}{12} - \frac{6EI}{l^2}u \\
Q_{AB} &= \frac{ql}{2} + \frac{12EI}{l^3}u
\end{aligned}
\right\}
\tag{6}
$$

Thus, the equation for the deflection curve of the AB part is given as

$$
y = \frac{qx^4}{24EI} - \left[\frac{ql}{2EI} + \frac{12}{l^3}u\right]\frac{x^3}{6} + \left[\frac{ql^2}{12EI} + \frac{6}{l^2}u\right]\frac{x^2}{2}
\tag{7}
$$

Eq. (7) shows that the softening effect of the relative humidity of the mine's atmosphere on the roof bed is mainly due to changes in the elastic modulus E. Therefore, to investigate the catastrophic instability mechanism of the pillar–roof system in a gypsum mine due to the softening effect of the relative humidity, Eq. (7) for the deflection of AB can be rewritten as Eq. (8) by considering the water-softening function $g_3'(w)$ of the elastic modulus E of the roof bed.

$$
y = \frac{qx^4}{24g_3'(w)EI} - \left[\frac{ql}{2g_3'(w)EI} + \frac{12}{l^3}u\right]\frac{x^3}{6} + \left[\frac{ql^2}{12g_3'(w)EI} + \frac{6}{l^2}u\right]\frac{x^2}{2}
\tag{8}
$$

In Fig. 2(c), the water-softening function $g_3'(w)$ of the elastic modulus E can be expressed as a linear function of the relative humidity ($R = 0.9965$).

Potential Function of the Support System

When the equilibrium position of the pillar–roof system experiences a quasi-static displacement u, the roof bed releases energy as each point in its flexural curve tends toward the static balance position illustrated in Fig. 5, and the energy released is called the elastic strain energy U_e. Additionally, the pillar generates a compressive deformation energy U_s because its upper end undergoes a compressive displacement u. This is the dissipation energy that can cause microfractures to extend and then connect in the pillars. The two energy components U_e and U_s are derived from the energy work performed by the equivalent uniform load q. Hence, the total potential function of the support system consists of the elastic strain energy U_e in the roof bed, the compressive deformation energy U_s in the pillar and the work W performed by the equivalent uniform load q; that is

$$
\Pi = -W + U_e + U_s
\tag{9}
$$

Combined with Eq. (8), the work W performed by the equivalent uniform load q is

$$
W = 2\int_0^l qy(x)dx = qlu + \frac{q^2l^5}{360g_3'(w)EI}
\tag{10}
$$

The elastic strain energy U_e of the roof bed is
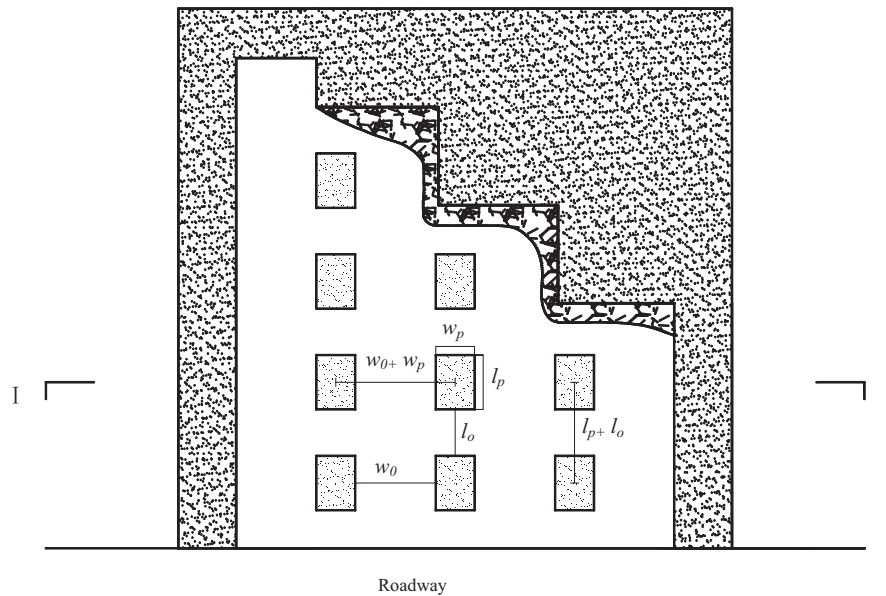
Fig. 3. Investigation of the distribution characteristics of the mined-out area in a gypsum mine.

$$U_e = g'_3(w)EI\int_0^l [\ddot{y}_1(x)]^2 dx = \frac{1}{g'_3(w)EI}\int_0^l \left\{ \frac{q^2 x^4}{4} - \left[\frac{q^2 l}{2} + \frac{12g'_3(w)EIq}{l^3}u\right]x^3 + \left[\frac{q^2 l^2}{3} + \frac{18g'_3(w)EIq}{l^2}u + \frac{144[g'_3(w)]^2 E^2 I^2}{l^6}u^2\right]x^2 \right.$$

$$\left. - \left[\frac{q^2 l^3}{12} + \frac{8g'_3(w)EIq}{l}u + \frac{144[g'_3(w)]^2 E^2 I^2}{l^5}u^2\right]x + \left[\frac{q^2 l^4}{144} + g'_3(w)EIqu + \frac{36[g'_3(w)]^2 E^2 I^2}{l^4}u^2\right] \right\} dx = \frac{q^2 l^5}{720 g'_3(w)EI} + \frac{12g'_3(w)EI}{l^3}u^2 \qquad (11)$$

When this is combined with Eq. (5), the compressive deformation energy U_s of the pillar is

$$U_s = \int_0^u F(u)du = \int_0^u g'_1(w)\lambda u \exp\left[-\left(\frac{u}{u_0}\right)^{g'_2(w)m}\right]du \qquad (12)$$

Substituting Eqs. (10)–(12) into Eq. (9), the total potential function of the support system Π can be obtained as

$$\Pi = \int_0^u g'_1(w)\lambda u \exp\left[-\left(\frac{u}{u_0}\right)^{g'_2(w)m}\right]du + \frac{12g'_3(w)EI}{l^3}u^2 - qlu$$
$$- \frac{q^2 l^5}{720 g'_3(w)EI} \qquad (13)$$

Cusp Catastrophe Model

Taking the compressive displacement u as the state variable, let $\Pi' = 0$; then, the equilibrium surface can be obtained based on the cusp catastrophe model

$$\Pi' = g'_1(w)\lambda u \exp\left[-\left(\frac{u}{u_0}\right)^{g'_2(w)m}\right] + \frac{24g'_3(w)EI}{l^3}u - ql \qquad (14)$$

Eq. (14) is the equilibrium equation for the stability analysis of the gypsum pillar–roof support system. As reported by Qin et al. (2001a, b,

2006), the standard cusp catastrophe model of the equilibrium surface does not include a u^2 term [Eq. (25)]. Therefore, it is necessary to identify the point at which the second derivative of $\Pi'(u)$ is 0, that is, the point at which $\Pi'''(u)$ is 0. Then, the Taylor series at this point, $\Pi'(u)$, does not include a u^2 term. Therefore, to obtain the standard cusp catastrophe model of the equilibrium surface, $\Pi'''(u)$ should be set to 0 (Qin et al. 2001b, 2006; Wang et al. 2006), that is

$$\Pi''' = -\frac{g'_2(w)m}{u_0}g'_1(w)\lambda \exp\left[-\left(\frac{u}{u_0}\right)^{g'_2(w)m}\right]\left(\frac{u}{u_0}\right)^{[g'_2(w)m-1]}$$

$$\times \left[g'_2(w)m + 1 - g'_2(w)m\left(\frac{u}{u_0}\right)^{g'_2(w)m}\right] = 0 \qquad (15)$$

From Eq. (15), the following is valid at the cusp:

$$u = u_1 = u_0\left[\frac{g'_2(w)m + 1}{g'_2(w)m}\right]^{1/[g'_2(w)m]} \qquad (16)$$

The point is called the cusp in catastrophe theory. Deriving the third-order Taylor series of Eq. (14) at the cusp u_1 and then, substituting Eq. (16) into Eq. (14) and simplifying yields
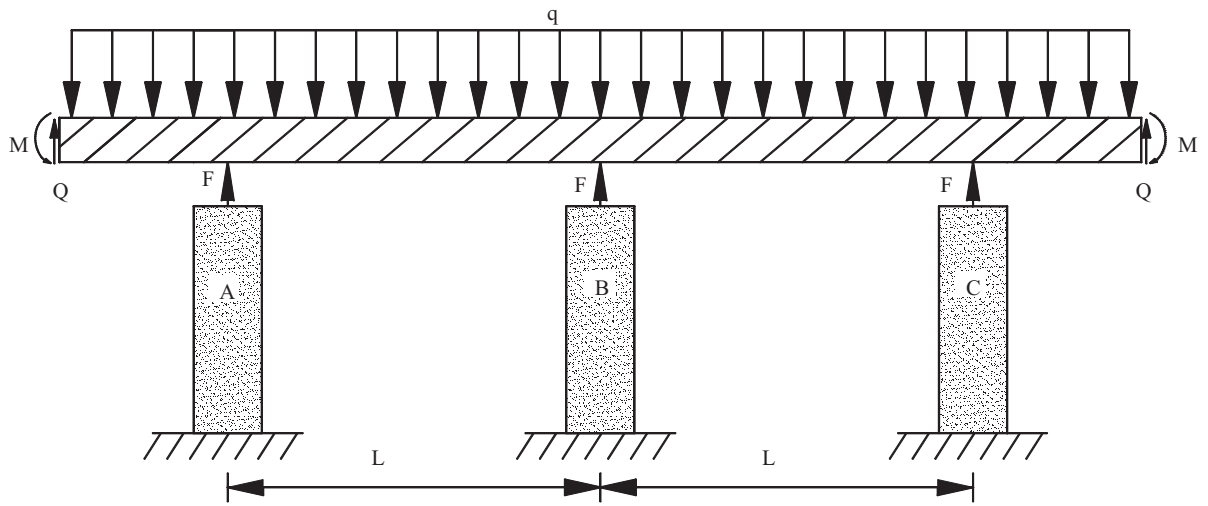
Fig. 4. Gypsum pillar–roof system under forces.
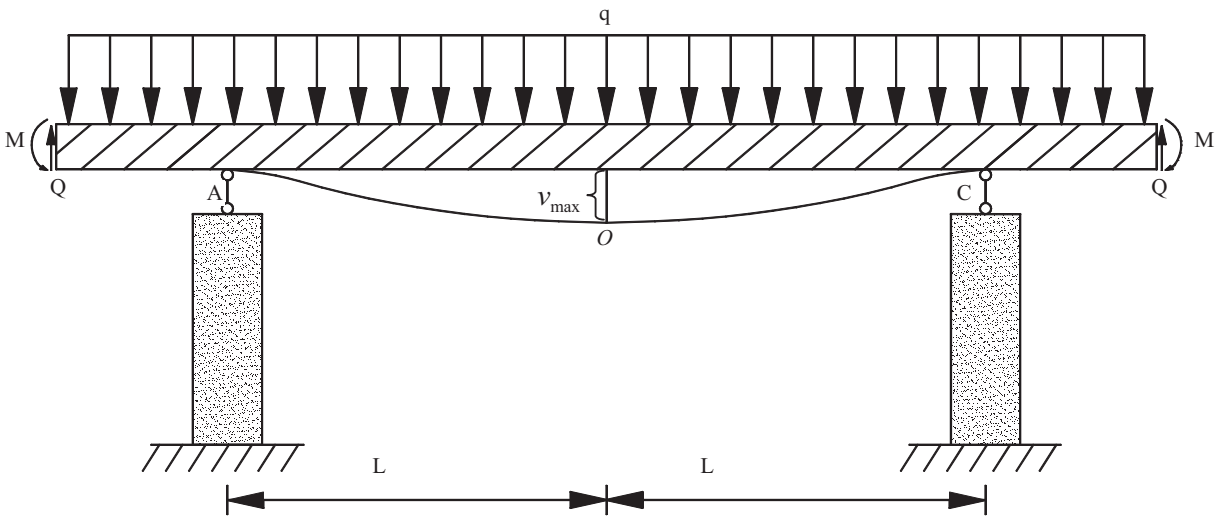
Fig. 5. Gypsum pillar–roof system without the support of pillar *B*.

Fig. 6. Moment and shear force at the end of the pillar.

$$\left(\frac{u - u_1}{u_1}\right)^3 + \frac{6}{[g_2'(w)m + 1]^2}\left\{\frac{24g_3'(w)EI/L^3}{\lambda g_1'(w)g_2'(w)m\exp\left[-\dfrac{g_2'(w)m + 1}{g_2'(w)m}\right]} - 1\right\}\left(\frac{u - u_1}{u_1}\right)$$

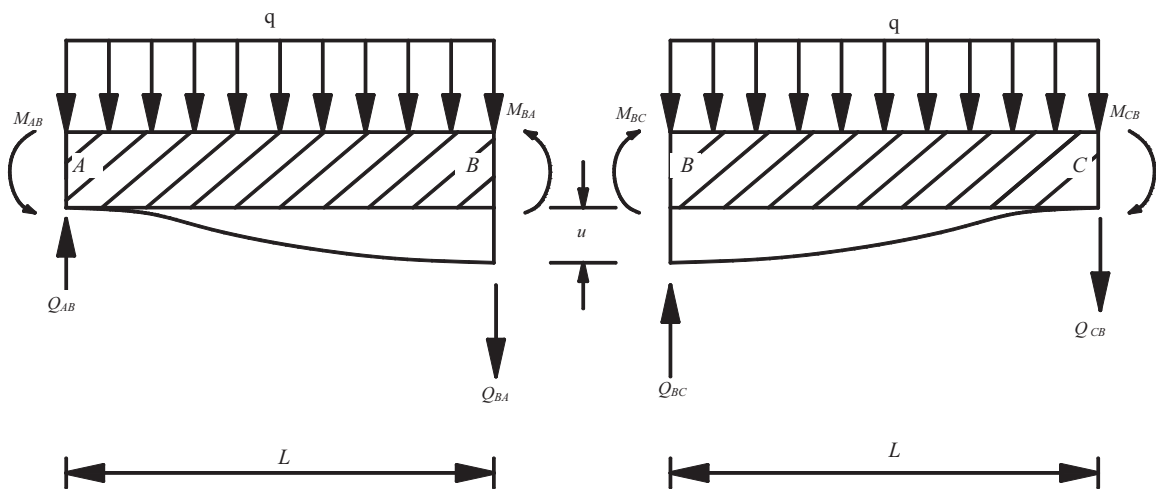$$+ \frac{6}{g_2'(w)m[g_2'(w)m + 1]^2}\left\{1 + \frac{24g_3'(w)EI/L^3}{\lambda g_1'(w)\exp\left[-\dfrac{g_2'(w)m + 1}{g_2'(w)m}\right]} - \frac{qL}{\lambda u_1 g_1'(w)\exp\left[-\dfrac{g_2'(w)m + 1}{g_2'(w)m}\right]}\right\} = 0 \qquad (17)$$

To transform Eq. (17) into the standard form of cusp catastrophe, let

$$x = \left(\frac{u - u_1}{u_1}\right) \qquad (18)$$

$$a = \frac{6}{[g_2'(w)m + 1]^2}(\eta - 1) \qquad (19)$$

$$b = \frac{6}{g_2'(w)m[g_2'(w)m + 1]^2}[1 + g_2'(w)m\eta - \xi] \qquad (20)$$

$$\eta = \frac{\eta_2}{\eta_1} = \frac{24g_3'(w)EI/L^3}{g_1'(w)\lambda g_2'(w)m\exp\left[-\dfrac{g_2'(w)m + 1}{g_2'(w)m}\right]} \qquad (21)$$

$$\xi = \frac{qL}{\lambda u_1 g_1'(w)\exp\left[-\dfrac{g_2'(w)m + 1}{g_2'(w)m}\right]} \qquad (22)$$

$$\eta_2 = \frac{24g_3'(w)EI}{L^3} \qquad (23)$$

$$\eta_1 = g_1'(w)g_2'(w)\frac{E_0 A}{H}m\exp\left[-\frac{g_2'(w)m + 1}{g_2'(w)m}\right] \qquad (24)$$

where η denotes the ratio of the flexural stiffness η_2 of the roof bed (also known as the local mine stiffness) to the absolute slope η_1 of the force-deformation curve for the gypsum pillar (hereafter referred to as the stiffness ratio).

Substituting Eqs. (18)–(24) into Eq. (17), the standard cusp catastrophe model of the equilibrium surface can be obtained as

$$x^3 + ax + b = 0 \qquad (25)$$

where x denotes its canonical state variable and a, b denote its canonical control parameters.

The standard cusp catastrophe model has the folded surface shape (as presented in Fig. 7), where the axes of the 3D space are the state variable x (vertical) and the control parameters a and b (horizontal). The projection of the fold point in the control plane is defined as the bifurcation set (Fig. 7). As reported by Thom (1972), the function of the bifurcation set can be expressed as

$$D = 4a^3 + 27b^2 = 0 \qquad (26)$$

Substituting Eqs. (19) and (20) into Eq. (26) yields

$$D = 4\beta^3(\eta - 1)^3 + 27\frac{\beta^2}{[g_2'(w)m]^2}[1 + g_2'(w)m\eta - \xi]^2 = 0 \qquad (27)$$

where $\beta = 6/[g_2'(w)m + 1]^2$

Catastrophe Mechanisms under the Influence of Relative Humidity

Necessary Condition for Catastrophe

Eq. (27) illustrates that the condition of $D = 0$ may be satisfied, that is, a catastrophic jump likely occurs, only when $\eta \leq 1$. Thus, in terms of $\eta \leq 1$, the necessary condition leading to catastrophe is

$$\eta = \frac{\eta_2}{\eta_1} = \frac{24g_3'(w)EI/L^3}{g_1'(w)\lambda g_2'(w)m\exp\left[-\dfrac{g_2'(w)m + 1}{g_2'(w)m}\right]} \leq 1 \qquad (28)$$

Clearly, a smaller stiffness ratio η of the support system results in a more unstable system. As reported by Hoek and Brown (1980), this is because if the pillar is in a region of low local mine stiffness, as in this case, catastrophic failure of the pillar occurs when, or shortly after, peak strength F_{max} is reached because the energy released by the mine is greater than the energy required to deform the pillar and excess energy is available to crash the pillar. However, if the pillar is in a region of high local mine stiffness, the roof is unable to supply the force necessary to deform the pillar beyond A and the situation is stable. In this case, controlled failure of the pillar (as opposed to violent catastrophic collapse) may occur. Therefore, the catastrophic analysis method based on the catastrophe model can significantly improve the traditional criterion for evaluating mine structure stability, and the traditional criterion considers only the peak strength of the gypsum rock at which the catastrophic failure occurs. However, the catastrophic failure of the pillar–roof system based on the catastrophe model depends on the relationship between the stiffness of the gypsum and the surrounding rock, which is reasonable.

Whether the stiffness ratio η decreases depends mainly on the change in the mechanical parameters of gypsum rock (i.e., the elastic modulus E, the initial elastic modulus E_0, and the brittleness index m) due to the relative humidity in the mine atmosphere through its physical and chemical action.

(1) When the relative humidity in the mine atmosphere increases around the pillars, the water-softening function $g_1'(w)$ of the initial elasticity modulus E_0 and the water-softening function $g_2'(w)$ of the brittleness index m both decrease. These decreases will lead to a larger stiffness ratio η of the support system and, consequently, a more stable support system, implying that an increase in the relative humidity around the

© ASCE

06019004-8

Int. J. Geomech.

pillars can reduce the potential for catastrophic accidents in the support system.

(2) When the relative humidity in the mine atmosphere increases around the roof bed, the water-softening function $g_3'(w)$ of the elasticity modulus E decreases. Thus, the stiffness ratio η of the support system decreases, thereby increasing the probability that the support system undergoes a catastrophic event.

(3) When the relative humidity in the mine atmosphere increases around both the pillars and the roof bed, that is, the water content of the pillar is equal to that of the roof bed. Through the analysis of the test data, the water-softening function $g_3'(w)$ is found to be approximately identical to the water-softening function $g_1'(w)$; as a result, Eq. (28) can be rewritten

$$\eta = \frac{24EI/L^3}{\lambda g_2'(w)m \exp\left[-\dfrac{g_2'(w)m + 1}{g_2'(w)m}\right]} \leq 1 \qquad (29)$$

In this case, the relative humidity in the mine atmosphere mainly influences the brittleness index m, and m gradually decreases. Such changes will result in a larger stiffness ratio η and thus in a more stable support system.

Stable and Unstable Regions in the Control Plane

As presented in Fig. 8, the control plane (a, b) can be divided into nine subsets: the shaded Regions III, IV, and OG "inside" the curve, the Regions I, II, and V "outside" the curve, the two branches OB_1 and OB_2 of the curve, and the origin O. When the control parameter (a, b) moves along different paths in the control plane, the stable state of the pillar–roof system lying in each region can be discussed as follows:

(1) When the control parameter (a, b) moves along path $B - B'$ in Fig. 7 and lies in Region I, as illustrated in Fig. 8, where $D > 0$

and $a > 0$, the system here is far from the critical state (bifurcation set), that is, the system is extremely stable.

(2) When the control parameter (a, b) is at the origin point o, where $a = 0$ and $b = 0$, this situation corresponds to the minimum relative humidity around the pillars and roof bed, leading to instability of the system and representing a particular point of instability (Qin et al. 2001a).

(3) When the control parameter (a, b) along path $A - A'$ moves to Region II, where $D > 0$, $b > 0$ and $a < 0$, Eq. (25) has only one real root; this situation corresponds to a minimum of the
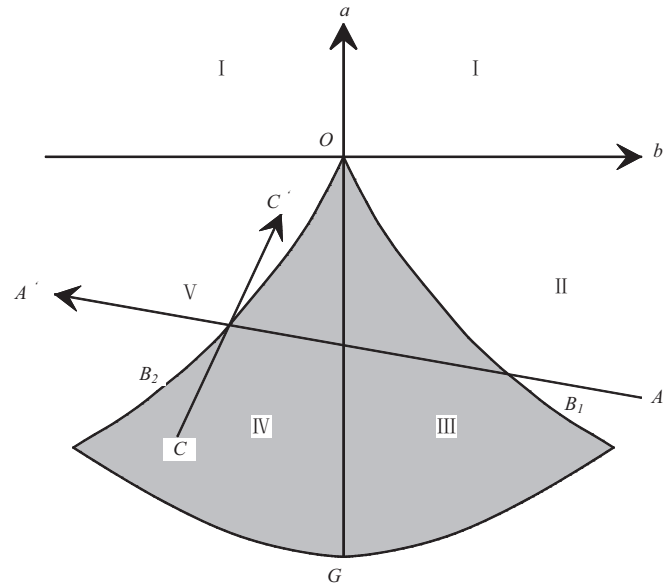

Fig. 8. Demarcation of the regions in the control plane by the bifurcation set.
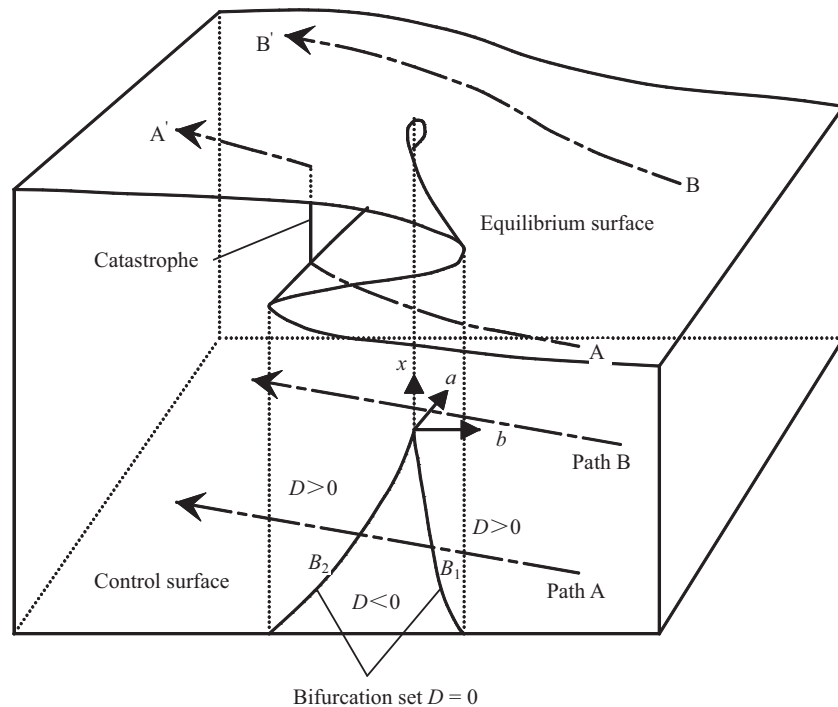

Fig. 7. Equilibrium surface of the cusp catastrophe model.

potential energy illustrated in Fig. 9(a) (Poston and Stewart 1978; Qin et al. 2001a). At this moment, the "dynamic effect" of the entire catastrophe system is a single valley and a smooth curve, and the state of the system will soon reach the valley bottom.

(4) When the relative humidity in the mine atmosphere gradually weakens the gypsum rock, the control parameter (a, b) can pass through the right branch OB_1 of the bifurcation set [Fig. 9 (b)] into Region III [Fig. 9(c)], where $D < 0$, $b > 0$, $a < 0$ and Eq. (25) has three distinct real roots. This corresponds to two minima on either side of a maximum of the potential energy. The small ball located at the first valley [Fig. 9(c)] cannot shift to the second valley because it is separated from the second valley by the peak and the first valley is far lower than the peak (Qin et al. 2001a). Thus, the relative humidity change around the pillars and roof bed does not cause instability in the gypsum pillar–roof support system.

(5) With further increases in the relative humidity of the mine atmosphere around the pillar and roof bed, the control parameter (a, b) enters Region IV [Fig. 9(e)] through OG [Fig. 9(d)], where $D < 0$, $b < 0$ and $a < 0$. At this moment, the second valley gradually deepens and then becomes deeper than the first valley. When the control parameter (a, b) approaches the edge of the fold, a slight change in the parameters can cause the small ball located at the first valley [Fig. 9(e)] to cross the peak and shift to the second valley. In other words, the perturbations can lead to a certain degree of instability of the support system.

(6) With considerable further increase in the relative humidity of the mine atmosphere, the control parameter (a, b) reaches the left branch OB_2 of the bifurcation set. Eq. (25) has one pair of duplicate real roots and a real root corresponding to an inflection point in the energy curve and a minimum of the energy [Fig. 9(f)]. Because the first valley is eliminated at the inflection point, the equilibrium of the system breaks down and suddenly moves to the new minimum (Qin et al. 2001a). Thus, the support system has been broken down in Region V [Fig. 9(g)]. It should be note that the support system passes through the bifurcation set; in addition to evolution path $A - A'$, other

evolution paths, such as $C - C'$, illustrated in Fig. 8, may occur. At this moment, the algebraic value of control parameters (a, b) gradually increases, that is, the control parameters (a, b) gradually converge to the values at the axis.

Based on this analysis, the state of the system can be subjected to a catastrophe only when the support system passes through the left branch of the bifurcation set, that is, when the sufficient and necessary condition leading to instability of the support system is

$$\left.\begin{array}{l} \dfrac{27}{\left[g_2'(w)m\right]^2}\left[1 + g_2'(w)m\eta - \xi\right]^2 + \dfrac{24}{\left[g_2'(w)m + 1\right]^2}(\eta - 1)^3 \geq 0 \\[2mm] 1 + g_2'(w)m\eta - \xi < 0 \\[2mm] \eta \leq 1 \end{array}\right\}$$
(30)

Eq. (30) shows that catastrophic instability of the support system is related not only to the geometric and mechanical parameters (i.e., I, L, A, H, E, E_0, and m) but also to the equivalent uniform load q. Hence, catastrophic instability of the support system is the comprehensive result both of its internal properties and of the external factors, and the influence of the relative humidity on the support system mainly involves a change in the mechanical parameters, including E, E_0, and m. Fig. 10 summarizes the method that was used in this study to investigate the catastrophic instability mechanism of the pillar–roof system in a gypsum mine due to the softening effect of relative humidity.

Case Study

The Jinghua Gypsum Mine considered in this case study is located in Jingmen City, Hubei Province, China. The thickness (89 m) of the overburden strata in this mine ranges from approximately 40 to 113 m. To improve the analysis of the catastrophic process, a thickness of 89 m was employed, and the other geometric design and physical parameters of the gypsum mine are shown in Table 3. Through *in situ* monitoring, the relative humidity of the mined-out area of this gypsum mine was known to be relatively constant at
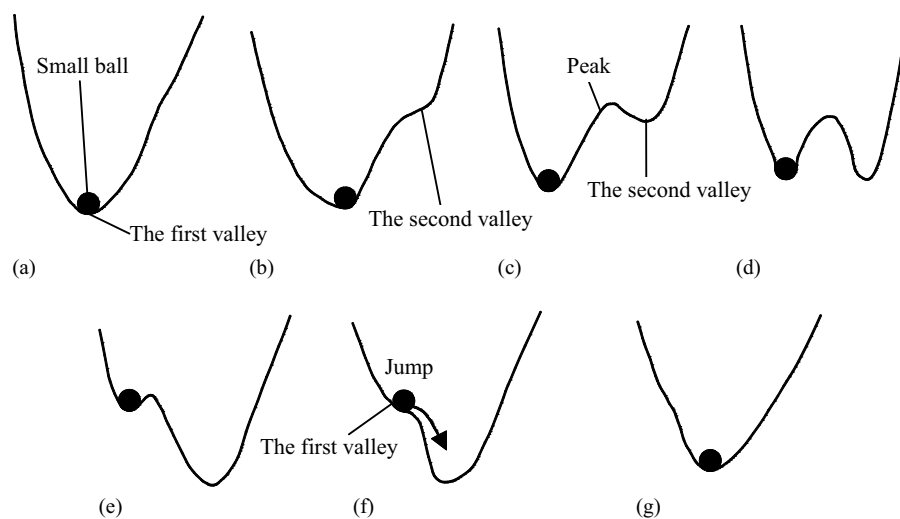
Fig. 9. Variation in the potential energy of the system as the relative humidity increases around the pillar and roof bed. (Modified from Qin et al. 2001a.) The curve and small ball represent the potential energy and the support system of the pillar–roof bed, respectively. The valley represents the local energy minimum, whereas the peak represents the local energy maximum. (a) ∈ Region II; (b) ∈ the right branch OB_1 of the bifurcation set; (c) ∈ Region III; (d) ∈ OG; (e) ∈ Region IV; (f) ∈ the left branch OB_2 of the bifurcation set; and (g) ∈ V in Fig. 9.
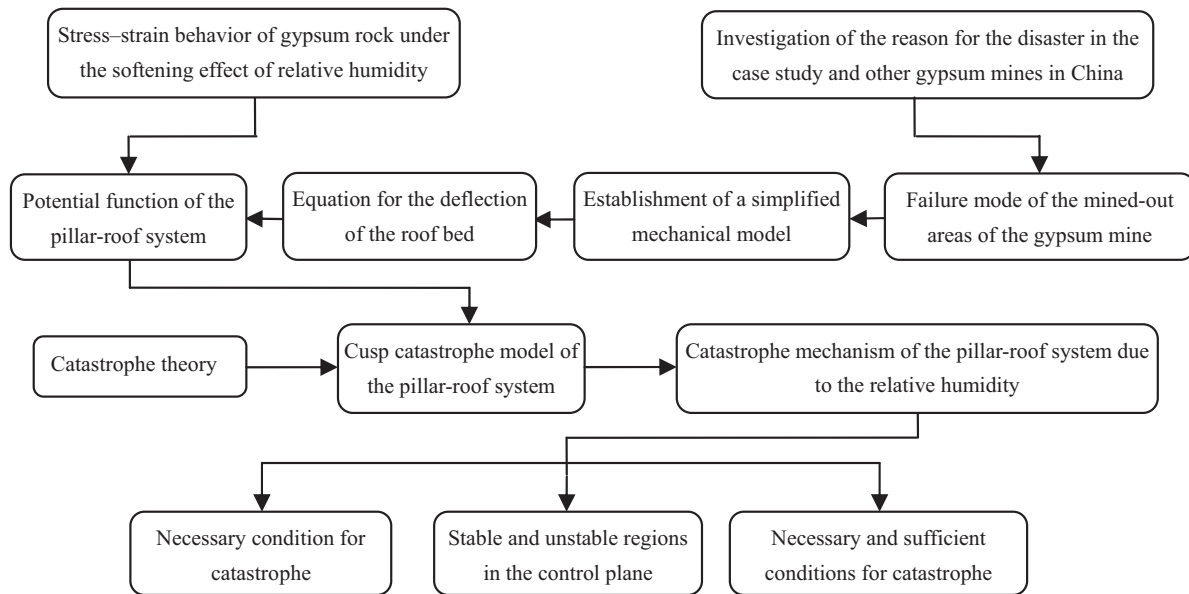
Fig. 10. Flowchart summarizing the method described in this study.

approximately 85%, and the natural and the extreme conditions (i.e., the pillars and roof bed both in the relative humidity of 100%) were taken into consideration in investigating the influence of relative humidity on the stability of the support system. (Hereafter, these conditions are referred to as the first, second, and third conditions in order of the magnitude of their relative humidities).

The magnitudes of the three expressions for the sufficient and necessary condition [i.e., Eq. (30)] under the aforementioned three conditions when the pillar spacing varies from 10.0 to 12.0 m (interval of 0.1 m) and the roof bed thickness varies from 1.5 to 3.5 m (interval of 0.1 m) are given in Tables 4 and 5.

The control parameter b for the sufficient and necessary condition [i.e., the second expression of Eq. (30)] revealed that the relative humidity mainly degrades the elastic modulus E, the initial elastic modulus E_0, and the brittleness index m to affect the control parameter b. Therefore, based on this analysis, the second term of control parameter b

$$\frac{24g_3'(w)EI/L^3}{\lambda g_1'(w)\exp\left[-\dfrac{g_2'(w)m+1}{g_2'(w)m}\right]}$$

typically increases with increasing relative humidity, and the third term of the control parameter b

$$\frac{qL}{\lambda u_1 g_1'(w)\exp\left[-\dfrac{g_2'(w)m+1}{g_2'(w)m}\right]}$$

may increase or decrease. Under the condition that the third term increases, whether the control parameter b increases mainly depends on the degrees to which the second and third terms increase. For example, under the first and second conditions, the extent of the increase of the third term is greater than that of the second term; thus, the control parameter b decreases, as illustrated in Tables 4 and 5. At this moment, the evolution path that the control parameters a, b of the support system take through the bifurcation set can be expressed in $A - A'$ with increasing environmental

Table 3. The design geometric parameters of the mined-out area in the Jinmen Gypsum Mine

Parameter	Value
Spacing [$L \times T$ (m)]	11×11
Thickness of roof bed [d (m)]	2.5
Pillar height [H (m)]	7
Cross sectional area of the pillar [A (m^2)]	4×4
Density of overburden strata [ρ (kg/m^3)]	2,400
Density of gypsum rock [ρ_0 (kg/m^3)]	2,316

humidity in the mined-out area. When the relative humidity in the mine atmosphere further weakens the support system, that is, the second condition changes to the third condition, the second term increases, whereas the third term decreases. As a result, the control parameter b of the third condition is greater than that of the second condition, as illustrated in Tables 4 and 5. In this case, the control parameter b remains greater than that of the first condition before the pillar spacing L reaches 11.6 m, and it becomes greater than that of the first condition when the roof bed thickness d exceeds 2.3 m. Moreover, the evolutionary path that the control parameters a, b of the support system take through the bifurcation set can be expressed in $C - C'$ with increasing environmental humidity in the mined-out area.

Based on the analysis of the control parameters a, b and discriminant D on each region of the control plane, the subdivided regions and the stability state of the support system under the aforementioned three conditions with variations in the pillar spacing and roof bed thickness are listed in Tables 4 and 5.

Tables 4 and 5 illustrate that under the given variation range of pillar spacing, the support system evidently remains in the stable state in the first condition. In the second condition, the support system begins to enter the unstable state when the pillar spacing is 11.3 m. In the third condition, the support system begins to enter the unstable state when the pillar spacing is 11.1 m. Under the given range of variation of the roof bed thickness, the support system remains in the stable state in the first condition. In the second condition, the support system is unstable when the roof bed thickness varies from 1.5 to 2.0 m. In the third condition, the support system

Table 4. Magnitudes of the necessary condition η, control parameter b, and discriminant D when the pillar spacing varies from 10.0 to 12.0 m (first through third conditions)

Pillar spacing [L (m)]	First condition				Second condition				Third condition			
	Necessary condition (η)	Control parameter (b)	Discriminant (D)	Stable state	Necessary condition (η)	Control parameter (b)	Discriminant (D)	Stable state	Necessary condition (η)	Control parameter (b)	Discriminant (D)	Stable state
10	0.1565	−0.0644	−2.0605	Region IV (stable state)	0.2249	−0.1520	−1.7436	Region IV (stable state)	0.4414	0.0005	−1.1587	Region IV (stable state)
10.1	0.1519	−0.0850	−2.0633		0.2183	−0.1751	−1.6777		0.4284	−0.0252	−1.2203	
10.2	0.1475	−0.1054	−2.0569		0.2119	−0.1978	−1.5958		0.4160	−0.0504	−1.2399	
10.3	0.1433	−0.1254	−2.0418		0.2058	−0.2202	−1.4983		0.4040	−0.0752	−1.2195	
10.4	0.1392	−0.1452	−2.0182		0.1999	−0.2423	−1.3860		0.3924	−0.0995	−1.1611	
10.5	0.1352	−0.1648	−1.9865		0.1942	−0.2641	−1.2593		0.3813	−0.1235	−1.0663	
10.6	0.1314	−0.1841	−1.9469		0.1888	−0.2856	−1.1188		0.3706	−0.1471	−0.9366	
10.7	0.1278	−0.2031	−1.8996		0.1836	−0.3068	−0.9648		0.3603	−0.1703	−0.7735	
10.8	0.1243	−0.2220	−1.8450		0.1785	−0.3279	−0.7979		0.3504	−0.1932	−0.5783	
10.9	0.1209	−0.2406	−1.7833		0.1736	−0.3486	−0.6183		0.3409	−0.2158	−0.3523	
11	0.1176	−0.2591	−1.7147		0.1689	−0.3692	−0.4266		0.3316	−0.2380	−0.0966	
11.1	0.1145	−0.2774	−1.6393		0.1644	−0.3895	−0.2230		0.3228	−0.2600	0.1878	Region V (unstable state)
11.2	0.1114	−0.2955	−1.5575		0.1601	−0.4096	−0.0079		0.3142	−0.2817	0.4998	
11.3	0.1085	−0.3134	−1.4692		0.1558	−0.4295	0.2185	Region V (unstable state)	0.3059	−0.3031	0.8386	
11.4	0.1057	−0.3311	−1.3748		0.1518	−0.4493	0.4559		0.2979	−0.3242	1.2033	
11.5	0.1029	−0.3487	−1.2743		0.1479	−0.4688	0.7040		0.2902	−0.3451	1.5931	
11.6	0.1003	−0.3662	−1.1678		0.1441	−0.4882	0.9625		0.2828	−0.3658	2.0072	
11.7	0.0977	−0.3835	−1.0557		0.1404	−0.5074	1.2313		0.2756	−0.3862	2.4450	
11.8	0.0953	−0.4006	−0.9378		0.1369	−0.5264	1.5102		0.2687	−0.4064	2.9059	
11.9	0.0929	−0.4176	−0.8145		0.1334	−0.5453	1.7988		0.2619	−0.4265	3.3892	
12	0.0906	−0.4345	−0.6857		0.1301	−0.5641	2.0971		0.2554	−0.4463	3.8944	

Int. J. Geomech.

Table 5. Magnitudes of the necessary condition η, control parameter b, and discriminant D when the roof bed thickness varies from 1.5 to 3.5 m (first through third conditions)

Roof bed thickness [d (m)]	First condition				Second condition				Third condition			
	Necessary condition (η)	Control parameter (b)	Discriminant (D)	Stable state	Necessary condition (η)	Control parameter (b)	Discriminant (D)	Stable state	Necessary condition (η)	Control parameter (b)	Discriminant (D)	Stable state
1.5	0.0254	−0.3929	−1.6503	Region IV (stable state)	0.0365	−0.5246	0.3385	Region V (unstable state)	0.0716	−0.4558	1.6056	Region V (unstable state)
1.6	0.0308	−0.3856	−1.6547		0.0443	−0.5161	0.2956		0.0869	−0.4436	1.5001	
1.7	0.0370	−0.3772	−1.6606		0.0531	−0.5063	0.2442		0.1043	−0.4297	1.3758	
1.8	0.0439	−0.3676	−1.6679		0.0631	−0.4951	0.1844		0.1238	−0.4137	1.2333	
1.9	0.0516	−0.3566	−1.6762		0.0742	−0.4823	0.1163		0.1456	−0.3957	1.0733	
2	0.0602	−0.3442	−1.6852		0.0865	−0.4680	0.0403		0.1698	−0.3756	0.8973	
2.1	0.0697	−0.3304	−1.6942		0.1001	−0.4519	−0.0430	Region IV (stable state)	0.1966	−0.3531	0.7079	
2.2	0.0801	−0.3151	−1.7026		0.1151	−0.4341	−0.1327		0.2260	−0.3282	0.5083	
2.3	0.0916	−0.2981	−1.7095		0.1316	−0.4144	−0.2276		0.2582	−0.3008	0.3033	
2.4	0.1041	−0.2795	−1.7140		0.1495	−0.3928	−0.3262		0.2934	−0.2708	0.0990	
2.5	0.1176	−0.2591	−1.7147		0.1689	−0.3692	−0.4266		0.3316	−0.2380	−0.0966	Region IV (stable state)
2.6	0.1323	−0.2369	−1.7103		0.1900	−0.3434	−0.5264		0.3730	−0.2024	−0.2733	
2.7	0.1482	−0.2128	−1.6990		0.2128	−0.3155	−0.6228		0.4178	−0.1637	−0.4185	
2.8	0.1652	−0.1867	−1.6789		0.2374	−0.2853	−0.7123		0.4659	−0.1220	−0.5165	
2.9	0.1836	−0.1586	−1.6477		0.2637	−0.2527	−0.7908		0.5177	−0.0771	−0.5480	
3	0.2032	−0.1283	−1.6029		0.2919	−0.2177	−0.8536		0.5731	−0.0288	−0.4896	
3.1	0.2242	−0.0959	−1.5414		0.3221	−0.1801	−0.8950		0.6323	0.0229	−0.3131	Region III (stable state)
3.2	0.2466	−0.0612	−1.4600		0.3543	−0.1400	−0.9084		0.6955	0.0781	0.0157	Region II (stable state)
3.3	0.2705	−0.0242	−1.3548		0.3886	−0.0971	−0.8865		0.7628	0.1370	0.5371	
3.4	0.2958	0.0153	−1.2214		0.4250	−0.0514	−0.8204		0.8342	0.1997	1.2993	
3.5	0.3227	0.0572	−1.0552		0.4636	−0.0029	−0.7001		0.9100	0.2663	2.3592	

is unstable when the roof bed thickness varies from 1.5 to 2.4 m. Hence, the influence of the relative humidity on the support system is significant, that is, as the relative humidity in the mine atmosphere further increases, there is a greater probability of instability of the support system.

To investigate the degree of influence of the relative humidity change around the roof bed and pillars on the system stability, the relative humidity around the pillars or roof bed is changed based on the first condition, that is, the relative humidity around the roof bed changes from the natural condition to a relative humidity of

Table 6. Magnitudes of the necessary condition η, control parameter b, and discriminant D when the pillar spacing varies from 10.0 to 12.0 m (fourth and fifth conditions)

Pillar spacing [L (m)]	Fourth condition				Fifth condition			
	Necessary condition (η)	Control parameter (b)	Discriminant (D)	Stable state	Necessary condition (η)	Control parameter (b)	Discriminant (D)	Stable state
10	0.1365	−0.0968	−2.1601	Region IV (stable state)	0.5063	0.0589	−0.6846	Region IV (stable state)
10.1	0.1325	−0.1165	−2.1484		0.4914	0.0315	−0.8416	
10.2	0.1286	−0.1359	−2.1284		0.4771	0.0046	−0.9499	
10.3	0.1249	−0.1551	−2.1006		0.4633	−0.0217	−1.0119	
10.4	0.1213	−0.1740	−2.0650		0.4501	−0.0476	−1.0300	
10.5	0.1179	−0.1928	−2.0220		0.4374	−0.0730	−1.0064	
10.6	0.1146	−0.2113	−1.9719		0.4251	−0.0980	−0.9429	
10.7	0.1114	−0.2296	−1.9148		0.4133	−0.1226	−0.8415	
10.8	0.1083	−0.2477	−1.8509		0.4019	−0.1468	−0.7037	
10.9	0.1054	−0.2657	−1.7805		0.3910	−0.1707	−0.5311	
11	0.1025	−0.2835	−1.7036		0.3804	−0.1941	−0.3252	
11.1	0.0998	−0.3011	−1.6206		0.3702	−0.2173	−0.0872	
11.2	0.0971	−0.3185	−1.5315		0.3604	−0.2401	0.1817	Region V (unstable state)
11.3	0.0946	−0.3358	−1.4365		0.3509	−0.2626	0.4802	
11.4	0.0921	−0.3530	−1.3357		0.3417	−0.2848	0.8074	
11.5	0.0897	−0.3700	−1.2292		0.3329	−0.3067	1.1622	
11.6	0.0874	−0.3869	−1.1172		0.3244	−0.3284	1.5438	
11.7	0.0852	−0.4037	−0.9997		0.3161	−0.3498	1.9513	
11.8	0.0831	−0.4203	−0.8770		0.3081	−0.3709	2.3839	
11.9	0.0810	−0.4369	−0.7490		0.3004	−0.3918	2.8409	
12	0.0790	−0.4533	−0.6158		0.2930	−0.4125	3.3216	

Table 7. Magnitudes of the necessary condition η, control parameter b, and discriminant D when the roof bed thickness varies from 1.5 to 3.5 m (fourth and fifth conditions)

Thickness of roof bed [d (m)]	Fourth condition				Fifth condition			
	Necessary condition (η)	Control parameter (b)	Discriminant (D)	Stable state	Necessary condition (η)	Control parameter (b)	Discriminant (D)	Stable state
1.5	0.0221	−0.3981	−1.6400	Region IV (stable state)	0.0822	−0.4463	1.4996	Region V (unstable state)
1.6	0.0269	−0.3920	−1.6426		0.0997	−0.4321	1.3738	
1.7	0.0322	−0.3849	−1.6467		0.1196	−0.4159	1.2282	
1.8	0.0383	−0.3767	−1.6524		0.1420	−0.3974	1.0634	
1.9	0.0450	−0.3673	−1.6593		0.1670	−0.3765	0.8814	
2	0.0525	−0.3567	−1.6671		0.1948	−0.3531	0.6846	
2.1	0.0608	−0.3449	−1.6756		0.2255	−0.3271	0.4771	
2.2	0.0699	−0.3317	−1.6841		0.2592	−0.2983	0.2640	
2.3	0.0798	−0.3171	−1.6921		0.2962	−0.2667	0.0526	
2.4	0.0907	−0.3010	−1.6989		0.3365	−0.2320	−0.1477	Region IV (stable state)
2.5	0.1025	−0.2835	−1.7036		0.3804	−0.1941	−0.3252	
2.6	0.1153	−0.2643	−1.7052		0.4279	−0.1530	−0.4645	
2.7	0.1292	−0.2435	−1.7024		0.4792	−0.1085	−0.5470	
2.8	0.1441	−0.2209	−1.6939		0.5344	−0.0604	−0.5494	
2.9	0.1601	−0.1966	−1.6779		0.5937	−0.0086	−0.4433	
3	0.1772	−0.1704	−1.6525		0.6573	0.0470	−0.1940	Region III (stable state)
3.1	0.1955	−0.1424	−1.6158		0.7253	0.1065	0.2402	Region II (stable state)
3.2	0.2150	−0.1123	−1.5651		0.7977	0.1701	0.9096	
3.3	0.2358	−0.0802	−1.4977		0.8749	0.2379	1.8739	
3.4	0.2579	−0.0460	−1.4105		0.9568	0.3101	3.2043	
3.5	0.2814	−0.0097	−1.2999		1.0438	0.3867	4.9849	Region I (stable state)

100% (hereafter referred to as the fourth condition), and the relative humidity around the pillars changes from the natural condition to a relative humidity of 100% (hereafter referred to as the fifth condition). For these two conditions, the results are provided in Tables 6 and 7.

Tables 6 and 7 illustrate that small changes in the necessary condition η, control parameter b, and discriminant D occur when the relative humidity around the roof bed changes from the natural condition to a relative humidity of 100% (i.e., the first condition to the fourth condition) and the subdivided regions and the stability state of the support system are the same as in the first condition with the variation of the pillar spacing and roof bed thickness. Large changes in the necessary condition η, control parameter b, and discriminant D occur when the relative humidity around the pillars changes from the natural condition to a relative humidity of 100% (i.e., the first condition to the fifth condition). Meanwhile, the subdivided regions and the stability state of the support system will differ greatly from the first condition. Hence, the effect of the relative humidity change around the pillar on system instability is greater than that around the roof bed.

Conclusions

The following conclusions can be obtained from the analysis of the instability mechanism for the pillar–roof system in gypsum mines using the catastrophe model that considers the influence of relative humidity.

- The stress–strain relation of gypsum rock derived from damage mechanics theory can accurately describe its strain-softening property after peak stress, and the average strain ε_0 remains nearly unchanged. However, the initial elastic modulus E_0 and brittleness index m gradually decrease with an increase in the relative humidity in the mine atmosphere; thus, the constitutive relationship of the gypsum rock is improved in these two respects.
- The catastrophic failure of the support system depends upon the relationship between the stiffness of the gypsum and that of the surrounding rock. Increases in the relative humidity around a pillar or around both a pillar and the roof bed will lead to a larger stiffness ratio of the support system and thus a more stable support system. However, as the relative humidity around the roof bed increases, the stiffness ratio of the system decreases, making it more likely that the support system will undergo a catastrophic event.
- Catastrophic instability of the support system is the comprehensive result of both its internal properties and external factors, and the influence of the relative humidity on the support system is mainly a change in its mechanical parameters. This case study shows that the influence of relative humidity on the support system is significant, that is, the probability that instability of the support system occurs increases as the relative humidity in the mine atmosphere continues to increase, and the influence of the relative humidity change around the pillar on system stability is greater than that around the roof bed.
- The catastrophic instability method based on the catastrophe model described in this study is applicable to the gypsum pillar–roof system, and it can significantly improve the traditional criterion for evaluating the mine structure stability. The traditional criterion considers only the peak strength of the gypsum rock at which the catastrophic failure occurs.

References

Auvray, C., F. Homand, and D. Hoxha. 2008. "The influence of relative humidity on the rate of convergence in an underground gypsum mine." *Int. J. Rock Mech. Min. Sci.* 45 (8): 1454–1468. https://doi.org/10.1016/j.ijrmms.2008.02.008.

Auvray, C., F. Homand, and C. Sorgi. 2004. "The aging of gypsum in underground mines." *Eng. Geol.* 74 (3–4): 183–196. https://doi.org/10.1016/j.enggeo.2004.03.008.

Bertolini, L., M. Carsana, and M. Spada. 2010. "Filling of a flooded gypsum mine with a flowable soil-cement mix." *J. Mater. Civ. Eng.* 22 (6): 628–636. https://doi.org/10.1061/(ASCE)MT.1943-5533.0000084.

Castellanza, R., R. Nova, and G. Orlandi. 2010. "Evaluation and remediation of an abandoned gypsum mine." *J. Geotech Geoenviron Eng.* 136 (4): 629–639. https://doi.org/10.1061/(ASCE)GT.1943-5606.0000249.

Cheng, Y. F., L. Jiang, H. D. Wang, U. Ansari, Z. Y. Han, and J. Ding. 2017. "Experimental study on pore structure and mechanical properties of stratified coal." *Int. J. Geomech.* 17 (12): 04017116. https://doi.org/10.1061/(ASCE)GM.1943-5622.0001022.

Cui, X., Y. Gao, and D. Yuan. 2014. "Sudden surface collapse disasters caused by shallow partial mining in Datong coalfield, China." *Nat. Haz.* 74 (2): 911–929. https://doi.org/10.1007/s11069-014-1221-5.

Henley, S. 1976. "Catastrophe theory models in geology." *J. Int. Assoc. Math. Geol.* 8 (6): 649–655. https://doi.org/10.1007/BF01031095.

Hoek, E., and E. T. Brown. 1980. *Underground excavations in rock.* London: Institution of Mining and Metallurgy.

Hu, J. H., K. P. Zhou, X. B. Li, N. G. Yang, and J. H. Su. 2005. "Numerical analysis of application for induction caving roof." *J Cent. South Univ. Technol.* 12 (1): 146–149. https://doi.org/10.1007/s11771-005-0389-y.

Liu, C. L., Z. X. Tan, K. Z. Deng, and P. X. Li. 2013. "Synergistic instability of coal pillar and roof system and filling method based on plate model." *Int. J. Min. Sci. Technol.* 23 (1): 145–149. https://doi.org/10.1016/j.ijmst.2013.03.005.

Pan, Y., A. W. Li, and Y. S. Qi. 2009. "Fold catastrophe model of dynamic pillar failure in asymmetric mining." *Min. Sci. Technol. (China)* 19 (1): 49–57. https://doi.org/10.1016/S1674-5264(09)60010-7.

Poston, T., and I. Stewart. 1978. *Catastrophe theory and its applications.* London: Pitman.

Qin, S. Q., J. J. Jiao, and Z. G. Li. 2006. "Nonlinear evolutionary mechanisms of instability of plane-shear slope: Catastrophe, bifurcation, chaos and physical prediction." *Rock Mech. Rock Eng.* 39 (1): 59–76. https://doi.org/10.1007/s00603-005-0049-4.

Qin, S., J. J. Jiao, and S. Wang. 2001a. "A cusp catastrophe model of instability of slip-buckling slope." *Rock Mech. Rock Eng.* 34 (2): 119–134. https://doi.org/10.1007/s006030170018.

Qin, S. Q., J. J. Jiao, S. J. Wang, and H. Long. 2001b. "A nonlinear catastrophe model of instability of planar-slip slope and chaotic dynamical mechanisms of its evolutionary process." *Int. J. Solids Struct.* 38 (44–45): 8093–8109. https://doi.org/10.1016/S0020-7683(01)00060-9.

Saunders, P. T. 1980. *An introduction to catastrophe theory.* Cambridge, UK: Cambridge University Press.

Tang, C. 1997. "Numerical simulation of progressive rock failure and associated seismicity." *Int. J. Rock Mech. Min. Sci.* 34 (2): 249–261. https://doi.org/10.1016/S0148-9062(96)00039-3.

Thom, R. 1972. *Stabilité structurelle et morphogénése.* [In French.] Reading, MA: W. A. Benjamin.

Wang, G. Y., G. L. You, and Y. L. Xu. 2008a. Investigation on the Nanjing gypsum mine flooding. In *Geotechnical Engineering for Disaster Mitigation and Rehabilitation*, edited by H. Liu, A. Deng, and J. Chu, 920–930. Berlin: Springer.

Wang, J. A., X. C. Shang, and H. T. Ma. 2008b. "Investigation of catastrophic ground collapse in Xingtai gypsum mines in China." *Int. J. Rock Mech. Min. Sci.* 45 (8): 1480–1499. https://doi.org/10.1016/j.ijrmms.2008.02.012.

Wang, Q. Y., W. C. Zhu, T. Xu, L. L. Niu, and J. Wei. 2017. "Numerical simulation of rock creep behavior with a damage-based constitutive law." *Int. J. Geomech.* 17 (1): 04016044. https://doi.org/10.1061/(ASCE)GM.1943-5622.0000707.

Wang, S. Y., K. C. Lam, S. K. Au, C. A. Tang, W. C. Zhu, and T. H. Yang. 2006. "Analytical and numerical study on the pillar rockbursts mechanism." *Rock Mech. Rock Eng.* 39 (5): 445–467. https://doi.org/10.1007/s00603-005-0075-2.

Yilmaz, I. 2007. "GIS based susceptibility mapping of karst depression in gypsum: A case study from Sivas Basin (Turkey)." *Eng. Geol.* 90 (1–2): 89–103. https://doi.org/10.1016/j.enggeo.2006.12.004.

Yilmaz, I., and G. Yuksek. 2009. "Prediction of the strength and elasticity modulus of gypsum using multiple regression, ANN, and ANFIS models." *Int. J. Rock Mech. Min. Sci.* 46 (4): 803–810. https://doi.org/10.1016/j.ijrmms.2008.09.002.